Experimental transition probabilities for several spectral lines arising from the $5d^{10}$ 6s{8s, 7p, 5f, 5g} electronic configurations of Pb III

A. Alonso-Medina

Departamento de Física Aplicada, EUIT Industrial, Universidad Politécnica de Madrid, Ronda de Valencia 3, 28012 Madrid, Spain

ARTICLE INFO

Keywords:
Transition probabilities
Lead
Plasma diagnostic
Laser-induced plasma spectroscopy

ABSTRACT

Transition probabilities for 30 spectral lines, arising from the $5d^{10}$ 6s{8s, 7p, 5f, 5g} electronic configurations of Pb III (20 measured for the first time), have been experimentally determined from measurements of emission line intensities in a plasma lead induced by ablation with a Nd:YAG laser. The line intensities were obtained with the target placed in molecular argon at 6 Torr, recorded at a 400 ns delay from the laser pulse, which provides appropriate measurement conditions, and analysed between 200 and 700 nm. They are measured when the plasma reaches local thermodynamic equilibrium (LTE). The plasma under study had an electron temperature (T) of 21,400 K and an electron number density (N_e) of 7×10^{16} cm^{-3}. The influence of self-absorption has been estimated for every line, and plasma homogeneity has been checked. The values obtained were compared with previous experimental values and theoretical estimates where possible.

1. Introduction

Data on transition probabilities for spectral lines is needed for atomic structure studies, and also for applications to astrophysics, plasma modeling and laser physics as well as analysis techniques. In Astrophysics, due to the spectra recorded by the Goddard high-resolution spectrograph on the Hubble Space Telescope, atomic data for many ions are of increasing interest. The analysis of spectral lines of Pb III provides information about the physical condition of hot stars (see, for example, the Pb III and Pb IV resonance lines that have been detected in the Far Ultraviolet Spectroscopic Explorer spectra of hot subdwarf B (sdB) stars by Chayer et al. [1]).

There has been continuous interest in the determination of oscillator strengths, transition probabilities and radiative lifetimes of Pb III. Some experimental transition probabilities, and theoretical values of oscillator strengths, transition probabilities and of some lifetimes, in Pb III have been the subject of three previous works carried out by this author. On the experimental side, the ten transition probabilities in the Pb III spectrum were measured using a plasma-induced laser, in an atmosphere of argon at 12 Torr, under local thermodynamic equilibrium (LTE) conditions [2]. On the theoretical side, transition probabilities of 54 lines for the $5d^{10}6s^2$–$5d^{10}6snp$, $5d^{10}6sns$–$5d^{10}6snp$ and $5d^{10}6snd$–$5d^{10}6snp$ spectral lines of Pb III presented in Colón and Alonso-Medina [3] were obtained in intermediate coupling and using relativistic Hartree–Fork calculations. Also theoretical transition probabilities and oscillator strengths of 382 lines arising from $5d^96s^26p$, $5d^{10}$ 6snl, $5d^{10}6s^2$, $5d^{10}6p^2$, $5d^{10}6p7s$ and $5d^{10}6p6d$ configurations and some radiative lifetimes of Pb III were presented in Alonso-Medina et al. [4]; these values were obtained in intermediate coupling and using relativistic Hartree–Fock calculations including core polarization effects.

Optical oscillator strengths for transitions $6s^2\ ^1S_0$-$6s6p\ ^{1,3}P_1$ of Pb III have been calculated by Migdalek and Baylis [5,6] and Migdalek and Bojara [7], using relativistic Hartree–Fock calculations and including a potential model to represent core polarization. Also, using a multi-configuration relativistic random phase approximation (MRRPA), values of theoretical oscillator strengths were obtained by Chou and Huang [8]. Huang et al. [9] and Chou and Kuang [10] obtained new improved values of these oscillator strengths using the MRRPA approximation, but including the core polarization effects explicitly. In 2003, Glowascki and Migdalek [11] obtained values of these oscillator strengths using relativistic Dirac–Fork calculations, including a potential model.

In 1972, Andersen et al. [12] presented a beam-foil study of atomic lifetimes showing the spectral line at 104.89 nm of Pb III. Ansbacher et al. [13], in 1988, presented a new beam-foil lifetime analysis of $6s6p\ ^{1,3}P_1$, $6s6d\ ^1D_2$, $6s7s\ ^1S_0$ and $6p^2\ ^1D_2$ levels of Pb III and Pinnington et al. [14] presented lifetimes of $6s6p\ ^{1,3}P_1$, $6s6d\ ^3D_{2,3}$, $6s7s\ ^3S_1$ and $6p^2\ ^1D_2$. Curtis et al. [15] presented a beam-foil measurement for lifetimes in Pb III, including a critical evaluation of the available database. Recently, the 5d photoabsorption spectra of Pb III have been recorded using the dual laser plasma technique in the photon energy range 30–66 eV by Banahan et al. [16].

In this paper, a plasma generated from ablation laser on a lead surface was used as a spectral source, the local thermodynamic equilibrium (LTE) assumption is discussed and the plasma parameters, such as temperature, electron density and self-absorption effects, were determined as well. Thus, also the homogeneity of the plasma is studied.

This paper aims to provide new experimental values of transition probabilities of Pb III. We present the transition probabilities of 30 spectral lines (arising from $5d^{10}$ 6s8s, $5d^{10}$ 6s7p, $5d^{10}$ 6s5f and $5d^{10}$ 6s5g configurations); to our knowledge for 20 of these there are no experimental values available in the literature. The transition probabilities have been measured by determining the emission line intensity of laser-produced plasma carried out with a lead target of 99.99% purity placed in an argon atmosphere at 6 Torr and 400 ns after each laser light pulse, which provides appropriate measurement conditions. Relative values of the transition probabilities, with the LTE assumption, have been put on an absolute scale using a Boltzmann plot of temperature and relative line strength measurements by comparison with the relative strength of the 504.26 nm Pb II transition in Saha's equation. Uncertainties from different contributions are estimated. Results are in good agreement with previous measurements and calculations.

2. Experimental setup and details of the measurements

The experimental system is similar to that described in previous papers [2,17–25], as more detailed description is presented in [17], only a brief description is given here. A diagram of the experimental device is shown in Fig. 1.

A focused Nd:YAG laser beam was used to generate the plasma on the surface of a lead target in a controlled argon atmosphere, and the plasma was employed as a source of Pb III ions. The light emitted by the laser-produced plasma was transmitted through a sapphire window to the entrance slit of a monochromator. The spectra were recorded by a time-resolved optical multichannel analyzer (OMA) that allowed recording of spectral regions at different delays after the laser pulse and during a selected time interval. The characteristics of the apparatus employed are shown in Table 1. To set the conditions, the experiment used a design programme for acquiring the data set: the number of spectra to be stored, the number accumulated in each reading and the time windows.

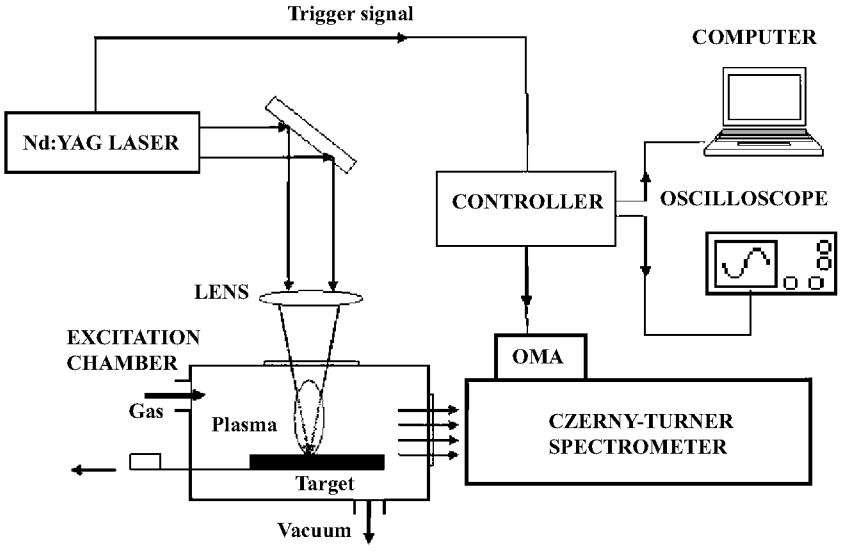

Fig. 1. Experimental setup used for obtained from relative line strength measurement.

Table 1
Experimental setup and settings used in this paper.

Laser (pulsed Q-witched Nd:YAG big sky)	
Model	Quantel Y G 585
Pulse width	7 ns
Energy	290 mJ
Wavelength	1064 nm
Repetition rate	20 Hz
Spectrometer and detection system	
Spectrometer (Spex 1704)	
Type	Czerny-Turner configuration (1 m focal length)
Grating	Holografic ruled 2400 grooves/mm
Slit widths (entrance)	50 μm
Detection system	
OMA III	EG&G PARC 1421 BHQ
Spectral response range	180–900 nm
Gate width	100–200 ns
Number of channels	1024-element linear silicon diode array
Quantumm efficiency	0.21 counts/photon in 3000 Å, 0.14 counts/photon in 5500 Å
Optics	
Focusing simple lens	Antireflection coated quartz, 12 cm focal length
Fiber optical cable	UV fused silica, incoherent bundle 1 m length, 1 mm diameter

The laser beam is deflected by total reflection in a prism and is focused, with a quartz lens of focal distance of 12 cm, on the surface of the target placed in position horizontally. Using a Q-switch Nd:YAG laser at 1064 nm, with a frequency of 20 Hz, a 7 ns nominal pulse width, an energy of 290 mJ/pulse and a spot size on the target of 0.5 mm resulted in an irradiance of 2×10^{10} W cm^{-2}. The laser energy was monitored using a calibrated power-meter.

A chamber was readied to generate the plasma with the target on a gas atmosphere, vacuum ($\sim 10^{-5}$ Torr) had already been attained inside the chamber by a turbo-molecular pump. The chamber was filled with argon and maintained at a constant pressure of 6 Torr throughout the measurement, using a small continuous flow of gas to maintain the purity of the atmosphere. The temperature, electron number density and time evolution of laser-produced plasma lead can be partially controlled by the use of a suitable buffer gas, and the buffer gas pressure value was chosen because it gives the best contrast between line emission and continuum emission. All the measurements that are presented here were performed in an argon atmosphere (6 Torr).

The chamber also has a target position-changing system, so the plasma is formed in each measurement on the smooth surface of the target and not on the crater that formed in the previous measurement. It features a quartz window that lets through light that is sent to the spectrometer entrance slit, located 8 cm from the plasma. The monochromator is Czerny-Turner type, in the range 190–700 nm, focal length of 1 m and a first-order resolution, for a slit of 50 μm, of 0.3 Å, which corresponds to 3 channels, a resolution that is hard to achieve, and equipped with a gated optical multichannel analyzer (OMA III EG&G) system, which can be used to record sections of the spectrum with a delay with respect to the laser pulse and for a selected interval of time. It has a time resolution, with a minimum duration of the time window of 100–200 ns, and the spectral band detected by the device is about 100 Å.

The measurements were repeated at several delay times (150–900 ns) and at a fixed gate time of 100 ns. The measurements consist in the accumulation of 20 laser pulses at a delay time. To obtain the best signal-to-noise ratio, the measurements of spectral lines of Pb III were made with a delay of 400 ns, and the recording interval was 100 ns. Fig. 2(a and b) presents two sections of typical spectra (in the range 433.5–442.5 and 363–371 nm wavelength, respectively) in a 6 Torr argon atmosphere, where some of the spectral lines of Pb I, Pb II, Pb III can be observed, and the corresponding most intense transitions of the Ar II and in these sections illustrate the temporal evolution of these spectral lines. In Fig. 2b, as the system is less efficient in this range, the Ar II lines are not observed. The detection was performed in a synchronized manner with the electronic device that regulates the laser Q-switch. The measurements were obtained after ablative cleaning the target for two laser pulses in order to remove impurities. In each data acquisition period, a correction was made with regard to the dark signal in the absence of the laser plasma. The instrumental line profile needed for the numerical analysis of each spectrum was determined from the observation of several narrow spectral lines from hollow-cathode lamps, with a precision of 97%. The distance at which two lines can be distinguished is 0.36 Å in first order.

The lines studied ranged from 200 to 700 nm. The system was calibrated in wavelength by recording the well-known lines of Ar, Ne and Hg covering the wavelength range 190–700 nm, and the uncertainties in the measurement were ≈ 0.001 Å. The calibration of the spectral response of the system (efficiency) was obtained

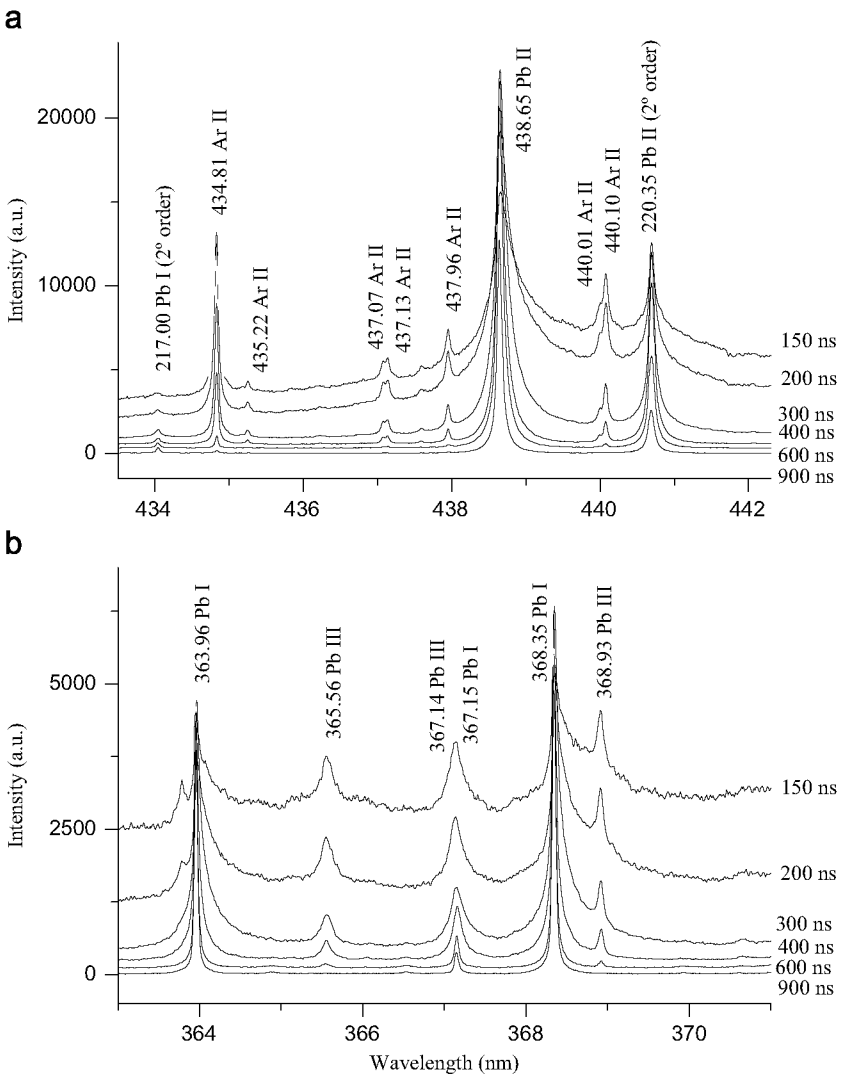

Fig. 2. (a) and (b). Emission spectra lines obtained for lead ablation (at 6 Torr in argon) at six delays: 150, 200, 300, 400, 600 and 900 ns. (a) The part of spectra in region 433–442 nm of Pb I, Pb II and Ar II lines. (b) The part of spectra in region 363–371 nm of Pb I and Pb III lines.

in the 200–700 nm wavelength range by means of previously calibrated lamps. A deuterium lamp was used for the 200–400 nm range, and a quartz–tungsten lamp for the 350–700 nm range. The final calibration was the result of the overlapping joint regions of these two lamps and also employing a least-square fitting process. The system efficiency was measured five times, and the error was estimated to be around 5%.

The same experimental system was used to study the homogeneity of the plasma, but in order to have spatial resolution, the light was focused by means of a lens on a 1 mm light guide being able to select the point of the plasma from which the light emission was observed, see schematic in Fig. 1 of Ref. [25]. The lens and optical fiber connector have been mounted on a telescopic spring that allows one to vary their relative distance to coincide with the focus distance of the plasma image, keeping the plasma–lens–optical fiber aligned. The support has been mounted on an optical bench, allowing controlled horizontal and vertical movements, thereby varying the area of plasma whose image is detected in the optical fiber.

The spectra were stored in a computer for further analysis and processed with software capable of separating two close overlapping lines and of determining their relative intensities, with uncertainties $\leq 3\%$. The spectra lines were analysed by fitting the observed line shapes to a numerically generated Voigt profile. This allows one to make the deconvolution to obtain the Lorentzian and Gaussian profiles, Lorentzian profile from Stark broadening, with Gaussian profile from Doppler broadening and instrumental broadening. For the plasma diagnostic, the area under each line profile from the aforementioned fitting represents the relative intensity. The line intensities were obtained by subtracting the background

intensity. Using spectral lines in a wider spectral range requires the measurement of various spectral regions, and this leads to the problem of assuring reproducibility between these measurements. In this paper, every result for the intensity was measured five times. The reason for not measuring more times was that the variation in the intensity values remained almost constant, so we obtained statistical uncertainty, ranging around 3% depending on each line. Local profiles were obtained after Abel inversion of the integrated intensity [26].

A major problem is self-absorption, which leads to a reduction in the intensities of the lines and has a great influence on the values of the transition probabilities. An estimation of the absorption coefficient of all the lines studied will be shown in a later discussion (Section 3.3), in order to verify that self-absorption was negligible. In this paper, self-absorption effects turned out to be lower than 1% for most intense lines. Thus, the plasma can be considered optically thin.

3. Results and discussion

A suitable choice of some spectral lines that are free from self-absorption allows the calculation of both temperature and density of the plasma.

3.1. Determination of the plasma temperature

When LTE conditions can be applied, the population of the linked states follows a Boltzmann distribution, which can be used as a first approximation to determine the temperature of the plasma [27,28]. The plasma temperature was measured using the Boltzmann plot for determining the excitation temperature, and Saha's equation was used for determining the ionization temperature. LTE plasmas are characterized by single temperature.

The excitation temperature can be determined by the well-known Boltzmann method, from relative line intensities (I_{ij}^{λ}), provided that their transition probabilities (A_{ij}) from a given excitation state are known from the same element and ionization stage. The basic principle of the Boltzmann plot is described below [27–29] by the expression

$$A_{ij} = \left(\frac{U(T)}{Ng_i}\right) I_{ij}^{\lambda} e^{E_i/kT}$$

$$\ln\left(\frac{I_{ij}^{\lambda}}{A_{ij}g_i}\right) = \ln\left(\frac{N}{U(T)}\right) - \frac{E_i}{kT} \quad (1)$$

for a transition from a higher state i to a lower state j, I_{ij}^{λ} represents the measured integral line intensity in counts s^{-1}, A_{ij} is the transition probability, λ the wavelength of the transition, E_i the excited level energy, g_i are the energy and statistical weight of level i, $U(T)$ is the atomic species partition function, N the total density of emitting atoms, k the Boltzmann constant (1.38×10^{-23} J/K) and T the temperature in K.

If we were to plot $\ln(I_{ij}^{\lambda}/g_iA_{ij})$ vs. E_i, for lines of known transition probability (Boltzmann plot), the resulting straight line would have a slope $-1/kT$, and therefore the temperature can be obtained without the need to know the total density of atoms or the atomic species partition function. The energies of the different levels are those of Moore [30].

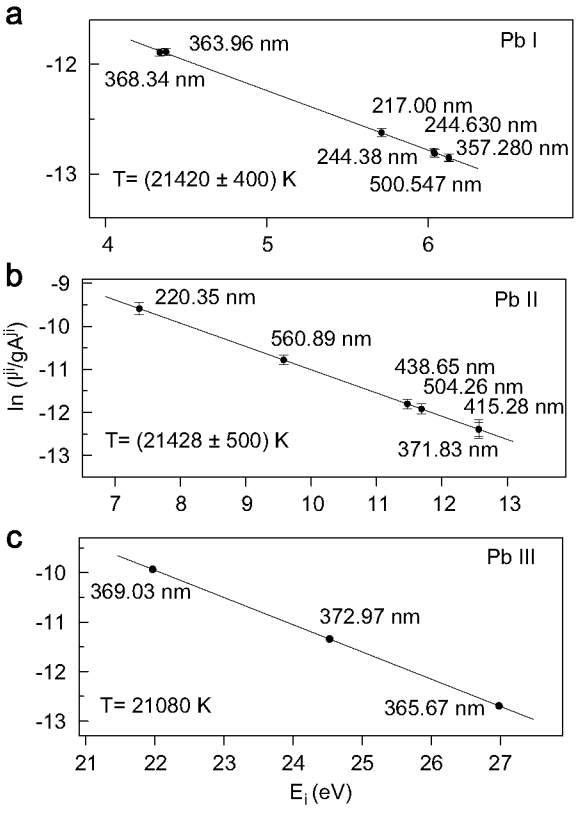

Fig. 3. (a–c). Boltzmann plots for Pb I, Pb II and Pb III spectral lines from laser-induced lead plasma, in argon at 6 Torr, were recorded at 400 ns delay time from laser pulse.

The excitation temperature has been determined by means of a Boltzmann plot for several lines of Pb I, obtaining 21,420 ± 400 K for ΔE=1.79 eV, of a Boltzmann plot for several lines of Pb II obtaining 21,428 ± 500 K for ΔE=5.19 eV and of a Boltzmann plot for several lines of Pb III obtaining 21,080 K for ΔE=5.02 eV, as can be seen in Fig. 3. These values were obtained from the relative intensities (I_{ij}^{λ}) required for applying this method, obtained using a laser-produced plasma in this paper, and the transition probabilities are as displayed in column four of Table 2 (values that were obtained in our previous studies [19,18,4] respectively). The errors were estimated from the standard deviation of the slopes obtained in the least squares fittings; the uncertainties that are taken into account are: (a) the line profile fitting procedure ($\leq$1%), (b) the relative line intensity determination ($\leq$2%) and (c) the transition probabilities (5–17%, depending on each line), see Table 2. All the data exhibited a linear fit with a correlation coefficient better than 0.999. Also, the excitation temperature was determined by means of a Boltzmann plot for three lines of Pb III ($5d^{10}$ 6s7p $^3P_0 \rightarrow$ $5d^{10}$ 6s7s $^3S_1$ at 479.99, $5d^{10}$ 6s7p $^3P_1 \rightarrow 5d^{10}$ 6s7s $^3S_1$ at 476.24 and $5d^{10}$ 6s7p $^3P_2 \rightarrow 5d^{10}$ 6s7s $^3S_1$ at 385.53 nm), and was found to be 21,400 ± 1500 K for small ΔE=0.63 eV. The reason for selecting these lines is that

Table 2
Spectroscopic parameters for selected Pb I, Pb II and Pb III spectral lines used to calculate the excitation temperature (at 6 Torr atmosphere Ar, delay time of 400 ns, the Pb target having a purity of 99.99%).

Species	Transition	λ (nm)[a]	E_i (eV)	A_{ij} (10^7 s^{-1})	Error (%)
Pb I	$7s\ ^3P_0 \rightarrow 6p^2\ ^3P_1$	368.35	4.336	16.76[b]	6.3
	$7s\ ^3P_1 \rightarrow 6p^2\ ^3P_1$	363.96	4.375	3.08[b]	6.8
	$6d\ ^3D_1 \rightarrow 6p^2\ ^3P_0$	217.00	5.712	17.29[b]	5.0
	$8s\ ^3P_1 \rightarrow 6p^2\ ^3P_1$	244.63	6.036	2.45[b]	6.1
	$8s\ ^3P_0 \rightarrow 6p^2\ ^3P_1$	244.38	6.041	4.93[b]	5.3
	$7s\ ^1P_1 \rightarrow 6p^2\ ^1D_2$	357.28	6.130	9.53[b]	6.3
	$7s\ ^1P_1 \rightarrow 6p^2\ ^1S_0$	500.55	6.130	0.85[b]	5.9
Pb II	$7s\ ^2S_{1/2} \rightarrow 6p\ ^2P_{3/2}$	220.35	7.370	49.30[b]	15
	$7p\ ^2P_{3/2} \rightarrow 7s\ ^2S_{1/2}$	560.89	9.580	8.48[c]	10
	$5f\ ^2F_{5/2} \rightarrow 6d\ ^2D_{3/2}$	438.65	11.472	15.57[c]	10
	$7d\ ^2D_{3/2} \rightarrow 7p\ ^2P_{1/2}$	504.26	11.689	9.00[c]	9.9
	$9s\ ^2S_{1/2} \rightarrow 7p\ ^2P_{3/2}$	415.28	12.565	2.23[c]	12.6
	$9s\ ^2S_{1/2} \rightarrow 7p\ ^2P_{1/2}$	371.83	12.565	1.20[c]	16.7
Pb III	$7p\ ^1P_1 \rightarrow 7s\ ^3S_1$	369.03	21.967	6.10[d]	
	$8s\ ^3S_1 \rightarrow 7p\ ^3P_1$	372.97	24.529	13.3[d]	
	$5g\ ^3G_3 \rightarrow 5f\ ^3F_2$	365.67	26.983	37.7[d]	

[a] Moore [30].
[b] Alonso-Medina et al. [19].
[c] Alonso-Medina [18].
[d] Alonso-Medina et al. [4].

the values of transition probabilities are experimentally known [2]. The linearity of the plots and the coincidence of the temperatures supported the existence of LTE.

The ionization temperature was calculated using the relative line intensity ratio method (in the electron density 7×10^{16} cm^{-3}), Saha's equation [26–28], between Pb I (217.00 and 500.55 nm) and Pb II (220.35 and 504.26 nm), and also between Pb II (371.83 nm) and Pb III (385.41 nm) spectral lines; the necessary atomic data are taken from Refs. [2,18,19]. The value obtained is 21,100 K with an estimated error of ~10%.

These values—the excitation temperature and the ionization temperature—are totally compatible and are close to 21,400 K, with an estimated error of ~7%.

3.2. Determination of the electron number density

As is well known, the shape and width of the spectral lines emitted by a plasma are governed by collisional processes of the emitting atoms and ions.

The electron number density of the plasma was determined, as in other papers [2,18–25,31–34], by comparing the Stark broadening for some transitions with those of other authors. As is well known, the Stark line broadening from collision of charged species is the primary mechanism influencing these emission spectra together with instrumental line broadening. The other mechanisms contributing to the line broadening, such as natural broadening, resonance broadening and Van der Waals broadening, are negligible at the range of the electron densities in this study [27,28]. However, an exact measurement of Stark broadening is not possible, unless the broadening of the spectral line due to the Doppler effect is considered.

A simple equation based on the Maxwellian distribution law can be used to estimate the full-width at half-maximum (FWHM) for Doppler broadening [26–28]

$$\omega_D(T) = \lambda_0 \sqrt{\frac{8kT \ln 2}{Mc^2}} \quad (2)$$

where λ_0 is the wavelength (m) at the centre of the absorption line, k the Boltzmann constant (J/K), T (K) the absolute temperature, M (kg) the atomic mass and c the speed of light (m/s). At a temperature of 21,400 K, the Doppler width is estimated to be $\approx$0.004 nm for the transition at 504.26 nm of Pb II and $\approx$0.003 nm for the transition at 385.41 nm of Pb III. This width is too small to be detected in the present work, and therefore is neglected.

The experimental profiles were fitted by a Voigt profile. As mentioned above, the Voigt profile is the convolution of a Lorentzian curve and Gaussian curve; spectral lines are thus Lorentzian-shaped. The Gaussian in the measured line profile is due to the spectroscopic apparatus. In this way convolution with the known instrumental profile can be taken into account, the spectral line intensity (area below profile) is obtained, the Lorentzian and Gaussian contributions to the full-width at half-maximum (FWHM) broadening can be separated and lines with partial overlapping can be analysed.

The FWHM of Stark broadening lines is related to the electron number density N_e (cm^{-3}) by the following expression [27–29]:

$$\omega = 2\omega_p \left(\frac{N_e}{10^{16}}\right) \left[1 + 1.75A \left(\frac{N_e}{10^{16}}\right)^{1/4} (1 - 1.2N_D^{-1/3})\right] \quad (3)$$

where ω (in Å) is the FWHM of the transition considered and obtained at the density N_e expressed in cm^{-3}, ω_p the Stark broadening parameter, A the ion broadening parameter and N_D the number of particles in the Debye sphere, which must be in excess of the lower limit N_D=2 of the Debye approximation for correlation effects [35]. For the electron densities present in this study, the quasi-static ion broadening, taken into account in the second term in expression (3), is only approximately 5% of the total width. In our measurements, we have assumed that A is negligible [36].

The electron number density, N_e, of the plasma under study is about 7×10^{16} cm^{-3} with an estimated error of ~13%, and has been obtained by comparing the Stark broadenings for several transitions with those of other authors, see Table 3. The error comes from the statistical uncertainties of measured line widths and the Stark widths taken from the literature [21–23]. We have selected lines, with published broadening Stark widths, that present small uncertainties: 385.41 and 538.01 nm Pb III spectral lines obtained in a previous work, for a temperature of 25,200 K and N_e=10^{17} cm^{-3}, Alonso-Medina and Colón [22]. The electron densities were $6.9 \pm 1.5 \times 10^{16}$ and $7.2 \pm 1.8 \times 10^{16}$ cm^{-3}, respectively. Also, we have selected other spectral lines, with published

Table 3
Electron density of lead plasma (at 6 Torr atmosphere Ar, delay time of 400 ns).

Species	Transition array	Multiplet	λ (nm)[a]	T (10^3 K)	ω_{exp} (Å)	N_e (10^{16} cm^{-3}) 21,400 K%
					$N_e=10^{17}$ cm^{-3}	
Pb I	$6p^2$–7s	$^3P_1$–$^3P_0$	368.35	11.2	0.131 ± 0.010[b]	6.8 ± 8
	$6p^2$–6d	$^3P_0$–$^3D_1$	217.00	11.2	0.108 ± 0.014[b]	7.0 ± 10
	$6p^2$–7s	$^1S_0$–$^1P_1$	500.55	11.2	0.075 ± 0.007[b]	6.8 ± 10
					$N_e=10^{16}$ cm^{-3}	
Pb II	6p–7s	$^2P_{3/2}$–$^2S_{1/2}$	220.35	11.3	0.11 ± 0.01[c]	7.3 ± 9
	6d–5f	$^2D_{3/2}$–$^2F_{5/2}$	438.65	11.3	0.13 ± 0.02[c]	7.2 ± 15
	7p–7d	$^2P_{1/2}$–$^2D_{3/2}$	504.26	11.3	0.39 ± 0.04[c]	7.1 ± 10
					$N_e=10^{17}$ cm^{-3}	
Pb III	7s–7p	$^3S_1$–$^3P_1$	385.41	25.2	0.75 ± 0.16[d]	6.9 ± 21
	6d–7p	$^3D_1$–$^3P_2$	538.01	25.2	2.7 ± 0.7[d]	7.2 ± 26

[a] Moore [30].
[b] Alonso-Medina [23].
[c] Colón and Alonso-Medina [21].
[d] Alonso-Medina and Colón [22].

broadening Stark, for Pb I and Pb II, see Table 3. The values of the electron densities obtained with such lines are in good agreement, and are values totally compatible with the value 7×10^{16} cm^{-3}. Also, the value of the electron number density has been confirmed by Saha's equation and is sufficient to assume LTE.

For the plasma to be in LTE, this requires the density to be high enough to ensure a high collision rate. The corresponding lower limit of electron number density is given by McWhirter's criterion [37]:

$$N_e(\mathrm{cm}^{-3}) \geq 1.6 \times 10^{12} \sqrt{T} (\Delta E)^3 \quad (4)$$

where ΔE (in eV) is the energy difference between the upper and the lower strongly radiatively coupled states, T (in K) the plasma temperature and N_e the lower limit of the electron density necessary to maintain the populations of the energy level at 10% of the LTE by collision, in completion with the radiative processes. Using the values obtained for the Pb I lines, the critical N_e is 1.35×10^{15} cm^{-3}; using the values obtained for the Pb II lines, the critical N_e is 3.28×10^{16} cm^{-3} and using the values obtained for Pb III lines, the critical N_e is 2.95×10^{16} and 5.84×10^{13} cm^{-3}.

The values given for N_e and T correspond to the centre of the plasma. To determine the change in these parameters in different regions of the plasma, we have obtained their values at different points using various lines of Pb III, and the result being that there is homogeneity for N_e and T.

3.3. Analysis of the self-absorption of the emission lines

Great care has been taken in this work to minimize the influence of self-absorption on emission line intensities determinations. The absence of self-absorption has been checked using a method described by Thorne [38].

With the aforementioned values of N_e and T we can calculate the absorption coefficient for the studied lines, expressed in m^{-1}

$$k_\omega = \frac{\pi e^2}{2\varepsilon_0 mc} f_{ik} N_i \left[1 - \frac{N_k g_i}{N_i g_k}\right] g(\omega) \quad (5)$$

where f_{ik} is the oscillator strength (absorption), g_i and g_j are statistical weight of state and $g(\omega)$ is the normalized profile of the line. In the maximum, $\omega=0$, and for a Lorentz profile, $g(0)=2/\pi\Gamma$, where Γ is the FWHM of the line. N_k and N_i, the population densities of the lower-level energy and the upper-level energy, respectively, were estimated at approximately equal to the electron density, this being an upper limit. A line may be considered optically thin if k_ω (cm^{-1}) $\times D$ (cm) $\ll 1$ [38,39]; in this work, $D \approx 1$ mm, the value of the optical depth $k_\omega D$ is not more than 0.1. The lines studied in this work self-adsorption was negligible.

3.4. Transition probabilities of Pb III spectral lines

In this paper, for homogeneous and optically thin plasma in LTE with the temperature $T=21{,}400 \pm 7\%$ K, the electron number density $N_e=7 \times 10^{16} \pm 13\%$ cm^{-3} and the relative line intensities measurements, the transition probabilities are obtained from the Boltzmann plot of temperature by expression (1) and, besides, with this temperature and this electron number density, from relative lines strength measurements by comparison with the relative line strength of the 504.26 nm Pb II transition of Saha's equation, have been confirmed. The uncertainties taken into account are: the line profile fitting procedure ($\leq 1\%$), the maximum intensity stability (2%), the self-absorption correction line errors ($< 1\%$), dispersion of temperatures obtained within the series of different diagnostics (7%), dispersion of electron density obtained within the different lines, see Table 3 and dispersion of the transition probability of the 504.26 nm of Pb II accuracy [18] (9.9%). Values obtained by these two methods are fully compatible. The total errors are about

Table 4
Experimental transition probabilities of several lines arising from $5d^{10}$ 6snl configurations of Pb III (in 6 Torr atmosphere Ar, delay time of 400 ns, lead target) obtained from the Boltzmann plot of temperature (21,400 ± 7% K). Comparison of the obtained values with some of the published ones.

Transition levels		λ (nm) (Moore [30])	Absolute transition probabilities (10^7 s^{-1})			
Upper	**Lower**		**This work**	**Colón et al. [2]**	**Alonso-Medina et al. [4]**	**Colón and Alonso-Medina [3]**
6s8s $^3S_1$	6s7p $^3P_0$	370.71	6.9 ± 0.83		6.0	
	6s7p $^3P_1$	372.97	14.3 ± 1.5		13.3	
	6s7p $^3P_2$	457.25	13.1 ± 1.4		11.4	
	6s7p $^1P_1$	482.82	2.0 ± 0.30		1.7	
	$5d^9$ $6s^2$6p $^1D_2$	500.34	1.9 ± 0.25		1.8	
6s8s $^3S_0$	6s7p $^3P_1$	353.12	11.0 ± 1.2		10.5	
	6s7p $^1P_1$	450.06	8.7 ± 1.0		7.1	
	$5d^9$6$s^2$6p $^3P_1$	403.23	16.5 ± 1.8		15.3	
	$5d^9$6$s^2$6p $^1P_1$	660.83	2.0 ± 0.32		2.2	
6s7p $^3P_0$	6s7s $^3S_1$	479.99	15.7 ± 1.7	17.2 ± 1.6	12.8	13.9
6s7p $^3P_1$	6s7s $^3S_1$	476.24	10.3 ± 1.0	11.9 ± 1.2	10.1	11.5
	6s7s $^1S_0$	578.10	9.2 ± 1.0	11.8 ± 1.2	1.2	1.8
	6s6d $^1D_2$	520.92	2.7 ± 0.35	3.6 ± 0.4	0.59	1.8
6s7p $^3P_2$	6s7s $^3S_1$	385.52	20.8 ± 2.1	21.1 ± 2.1	18.0	27.5
	6s6d $^1D_2$	414.28	0.93 ± 0.15	1.5 ± 0.2	0.01	0.03
	$6p^2$ $^3P_1$	485.64	0.86 ± 0.095	0.99 ± 0.13	0.000	
	6s6d $^3D_1$	538.25	0.26 ± 0.035	0.22 ± 0.02	0.25	0.19
	6s6d $^3D_2$	552.55	4.5 ± 0.45	6.3 ± 0.7	1.0	1.2
	6s6d $^3D_3$	585.97	6.9 ± 0.72	6.6 ± 0.6	6.0	7.4
6s7p $^1P_1$	6s7s $^3S_1$	369.03	7.0 ± 0.75		6.1	7.0
	6s6d $^1D_2$	395.30	0.88 ± 0.095		0.74	
	6s7s $^1S_0$	427.39	4.8 ± 0.55		4.2	15.5
	6s6d $^3D_1$	506.65	0.91 ± 0.15		0.81	
	6s6d $^3D_2$	519.31	2.5 ± 0.35		2.1	
6s5f $^3F_3$	6s6d $^3D_2$	313.87	34.2 ± 3.6		41.8	
6s5f $^3F_2$	6s6d $^3D_1$	304.47	36.8 ± 3.8		45.3	
6s5f $^3F_4$	6s6d $^3D_3$	317.74	39.6 ± 4.0		48.0	
6s5g$^3G_4$	6s5f $^3F_3$	359.09	31.6 ± 3.3		39.2	
6s5g$^3G_3$	6s5f $^3F_2$	365.67	27.5 ± 2.8		37.7	
6s5g$^1G_4$	6s5f $^3F_3$	373.70	28.6 ± 3.0		39.2	

10% for most of the studied transitions, except for the weakest lines whose errors are about 15% and for the results obtained from Saha's equation are about 20%.

Transition probabilities obtained for 30 spectral lines of Pb III with wavelengths in the range 300–700 Å are displayed in column three of Table 4, while columns one and two give the transitions and corresponding wavelengths, respectively. The remaining columns give the transition probability; the values are to be found in Refs. [2–4]. The values of column four have been measured in previous studies [2] and the values of columns five and six have been calculated in previous studies [3,4], respectively. We include the calculations of Ref. [4] because they provide transition probabilities of Pb III for all lines measured in this study.

The agreement is good except for some discrepancies. For example, line 552.55 nm the value obtained in this study is $4.5 \pm 0.4 \times 10^7\ s^{-1}$ compared to $6.3 \pm 0.7 \times 10^7\ s^{-1}$ obtained in Ref. [2]. In this work, are repeated the measured in the same working conditions (in an argon atmosphere at 6 Torr) five times.

4. Conclusions

Optical emission spectra of the plasma produced by the 10 640 Å Nd:YAG laser of lead sample in a 6 Torr argon atmosphere are recorded with a delay with respect to the laser pulse and for a selected interval of time, 400 ns. This study shows that laser-produced plasmas are a very interesting spectroscopic source but demanding time resolving spectroscopy for its study.

All the results presented in this work were obtained using a lead sample, having a purity of 99.99%. No self-absorption effects have been detected. The electron temperature of the plasma (21,400 K) has been determined from the Boltzmann plot method using the relative emission line intensities of Pb I, Pb II and Pb III and from Saha's equation, where the electron number density ($7 \times 10^{16}\ cm^{-3}$) is estimated from the Stark broadening profile of the spectral lines of Pb I, Pb II and Pb III. The LTE conditions have been checked.

Spectroscopy analysis of the plasma light emission has provided the experimental transition probabilities for 30 emission lines of Pb III. For 20 of these emission lines, no experimental values of transition probabilities have been made by other authors. A good agreement with previous reference data was found in almost all cases.

Acknowledgements

This work was supported in part by the project "PEL2G (CGL2008-06426-C01-01/BTE)" funded by the Spanish

Ministry of Science and in part by the project "MAT2008-02704/MAT" funded by the Spanish Ministry of Science and Technology.

References

[1] Chayer P, Fontaine M, Fontaine G, Wesemael F, Dupuis F. FUSE observations of germanium, zirconium and lead in sdB stars. Baltic Astron 2006;15:131–8.

[2] Colón C, Alonso-Medina A, Herrán-Martínez C. Spectroscopic study of a laser-produced lead plasma: experimental atomic transition probabilities for Pb III lines. J Phys B: At Mol Opt Phys 1999;32:3887–97.

[3] Colón C, Alonso-Medina A. Determination of theoretical transition probabilities for the Pb III spectrum. Phys Scr 2000;62: 132–6.

[4] Alonso-Medina A, Colón C, Zanón A. Core-polarization effects, oscillator strengths and radiative lifetimes of levels in Pb III. Mon Not R Astron Soc 2009;395:567–79.

[5] Migdalek J, Baylis WE. Relativistic Hartree–Fock oscillator strengths for the lowest s→p and p→d transitions in the first few members of the Ag(I) and Au(I) isoelectronic sequences, with allowance for cope polarization. J Quant Spectrosc Radiat Transfer 1979;22: 113–25.

[6] Migdalek J, Baylis WE. Relativistic oscillator strengths and excitation energies for the $ns^2\ ^1S_0$-$nsnp\ ^3P_1$, $^1P_1$ transitions: I. The mercury isoelectronic sequence. J Phys B: At Mol Opt Phys 1985;18:1533–47.

[7] Migdalek J, Bojara A. Relativistc CI calculations for the $ns^2\ ^1S_0$-$nsnp\ ^3P_1$, $^1P_1$ transitions in the cadmium and mercury isoelectronic sequences. J Phys B: At Mol Opt Phys 1988;21:2221–36.

[8] Chou H-S, Huang K-N. Relativistic excitation energies and oscillator strengths for the $6s^2\ ^1S_0$–$6s6p\ ^1P_1$, $^3P_1$ transitions in Hg-like ions. Phys Rev A 1992;45:1403–6.

[9] Huang K-N, Chi H-C, Chou H-S. The MCRRPA theory and its applications to photoexcitation and photoionization. Chin J Phys 1995;33:565–644.

[10] Chou H-S, Kuang K-N. Core-shielding effects on photoexcitation of the Hg-Like ions. Chin J Phys 1997;35:35–46.

[11] Glowascki L, Migdalek J. Relativistic configuration-interaction oscillator strength calculations with *ab inition* model potential wavefunctions. J Phys B: At Mol Opt Phys 2003;36:3629–36.

[12] Andersen T, Kirkegard A, Sorense G. A systematic study of atomic lifetimes of levels belonging to the Ag I, Au I, and Hg I isoelectronic sequences. Phys Scr 1972;6:122–4.

[13] Ansbacher W, Pinnington EH, Kernahan JA. Beam-foil lifetime measurements in Pb III and Pb IV. Can J Phys 1988;66:402–4.

[14] Pinnington EH, Ansbacher W, Kernahan JA, Ge Z-Q, Inamdar A-S. Beam-foil spectroscopy for ions of lead and bismuth. Nucl Instrum Methods Phys Res 1988;B31:206–10.

[15] Curtis LJ, Irving RE, Henderson M, Matulioniene R, Froese Fischer C, Pinnington EH. Measurements and predictions of the $6s6p\ ^{1,3}P_1$ lifetimes in the Hg isoelectronic sequence. Phys Rev A 2001;63:042502–042507.

[16] Banahan C, McGuinness C, Costello JT, Kilbane D, Mosnier J-P, Kennedy ET, et al. The 5d photoabsorption spectra of Pb III and Bi IV. J Phys B: At Mol Opt Phys 2008;41:205001 (9 pp).

[17] Alonso-Medina A. Probabilidades de transición en átomos pesados: aplicación al talio y al plomo. Razones de ramificación y momentos electrónicos de transición en la molécula de plata. Ph.D. Thesis 1995.Eindhove University Complutense of Madrid, Spain 2001: oai:www.ucm.es:1927. ISBN:84-669-0380-1.

[18] Alonso-Medina A. Transition probabilities of 30 Pb II lines of the spectrum obtained by emission of a laser-produced plasma. Phys Scr 1997;55:49–53.

[19] Alonso-Medina A, Colón C, Herrán-Martínez C. Experimentally determined transition probabilities for lines of Pb I and 2203.5 Å line of Pb II. J Quant Spec Radiat Transfer 2001;68:351–62.

[20] Alonso-Medina A, Colón C, Herrán-Martínez C. Transition from autoionized single-ionized tin status: a theoretical study of the $5s5p(^3P^0)nl(nl=5d,6s)$ levels of Sn II. Astrophys J 2003;595:550–4.

[21] Colón C, Alonso-Medina A. Application of a laser produced plasma: experimental Stark widths of single ionized lead lines. Spectrochim Acta Part B 2006;61:856–63.

[22] Alonso-Medina A, Colón C. Stark widths of several Pb III spectral lines in a laser-induced lead plasma. Astron Astrophys 2007;466: 399–402.

[23] Alonso-Medina A. Experimental determination of the Stark widths of Pb I spectral lines in a laser-induced plasma. Spectrochim Acta Part B 2008;63:598–602.

[24] Alonso-Medina A, Colón C. Measured Stark widths of several Sn I and Sn II spectral lines in a laser-induced plasma. Astrophys J 2008;672:1286–91.

[25] Alonso-Medina A. A spectroscopic study of laser-induced tin–lead plasma: transition probabilities for spectral lines of Sn I Spectrochim Acta Part B 2010;65:158–166.

[26] Lochte-Holtgreven W. In: Plasma diagnostics. North-Holland: WLochte-Holtgreven, Amsterdan; 1968.

[27] Griem HR. In: Plasma spectroscopy. New York: McGraw-Hill; 1964.

[28] Griem HR. In: Spectral line broadening by plasma. New York: Academic Press; 1974.

[29] Bekefi G. In: Principles of laser plasmas. New York: John Wiley & Sons; 1976.

[30] Moore CE, Atomic energy levels NBS 467, vol III 1958; U.S.GPO, Washington DC. p. 208.

[31] Shaikh N-M, Hafeez S, Rashid B, Baig MA. Spectroscopic studies of laser induced aluminium plasma using fundamental, second and third harmonics of a Nd:YAG laser. Eur Phys J D 2007;44:371–9.

[32] Le Drogoff B, Margot J, Chaker M, Sabsabi M, Barthélemy O, Johnston TW, et al. Temporal characterization of femtosecond laser pulses induced plasma for spectrochimical analysis of aluminium alloys. Spectrochim Acta Part B 2001;56:987–1002.

[33] Bengoechea J, Aguilera J-A, Aragón C. Application of laser-induced plasma spectroscopy to the measurement of Stark broadening parameters. Spectrochim Acta Part B 2006;61:69–80.

[34] Bredice F, Borges F-O, Sohal H, Villagran-Muniz M, Di Rocco HO, Cristoforetti G, et al. Measurement of Stark broadening of Mn I and Mn II spectral lines in plasmas used for laser-induced breakdown spectroscopy. Spectrochim Acta Part B 2007;62:1237–45.

[35] Wolf PJ. The plasma properties of laser-ablated SiO_2. J Appl Phys 1992;72:1280–9.

[36] Konjević N. Plasma broadening and shifting of non-hydrogenic spectral lines: present status and applications. Phys Rep 1999;316: 339–401.

[37] McWhirter RWP. In: Huddlestone RH, Leonard SL, editors. Plasma diagnostic techniques. New York: Academic Press; 1963.

[38] Thorne AP. In: Spectrophysics, 2nd edition. London: Chapman and Hall; 1988.

[39] Corney A. In: Atomic and Laser Spectroscopy. Oxford University Press; 1977.